ORNL/TM-1999/159

Stress Intensity Factors for HFIR HB-2 Nozzle Corner

P. T. Williams
B. R. Bass

ORNL/TM-1999/159

Stress Intensity Factors for HFIR HB-2 Nozzle Corner

P. T. Williams
B. R. Bass
Computational Physics and Engineering Division

Manuscript Completed – August 1999
Date Published – August 1999

Prepared by the
OAK RIDGE NATIONAL LABORATORY
Oak Ridge, Tennessee 37831-8056
managed by
LOCKHEED MARTIN ENERGY RESEARCH CORP.
for the
U. S. DEPARTMENT OF ENERGY
under Contract No. DE-AC05-96OR22464

CONTENTS

Page

LIST OF FIGURES iv

LIST OF TABLES v

ABSTRACT vii

1. INTRODUCTION 1

2. FINITE-ELEMENT MODELS 5
   2.1 GEOMETRY 5
   2.2 MATERIAL PROPERTIES 9
   2.3 THERMAL AND MECHANICAL LOADING 9
   2.4 ABAQUS QUALITY ASSURANCE 9
   2.5 STRESS INTENSITY FACTORS 11

3. RESULTS AND DISCUSSION 12

4. SUMMARY 12

ACKNOWLEDGMENTS 12

5. REFERENCES 16

LIST OF FIGURES

Figure **Page**

1. Vertical cross-section of HFIR pressure vessel including core, beryllium reflector, engineering facility, and beam tubes. 2
2. Horizontal cross-section of HFIR pressure vessel and core at horizontal midplane of core. 3
3. Present and new designs of HB-2 beam tube at nozzle location (from [1]). 4
4. Nozzle corner flaw with geometric variables defined (from [1]). 6
5. General mesh layout for 90 degree model of HB-2 corner flaw. 7
6. Mesh layouts of six corner flaws: (a) r_F = 0.25 in. (b) r_F = 0.5 in. (c) r_F = 0.75 in. (d) r_F = 1.0 in. (e) r_F = 1.25 in. (f) r_F = 1.5 in. 8
7. Contributions to maximum principal (opening-mode) stresses along nozzle-corner flaw front for flaw radii of (a) 0.5 in. and (b) 1.5 in. 10
8. Distribution of stress-intensity factors along flaw front for a range of flaw radii. 14
9. Stress intensity factors along flaw front with and without cladding for a flaw radius of 0.5 in. 14
10. Stress intensity factors along flaw front with and without cladding for a flaw radius of 1.5 in. 15

LIST OF TABLES

Table **Page**

Table 1. Corner Flaw Geometries.....5
Table 2. Material Properties 9
Table 3. Peak Stress Intensity Factors 12
Table 4. Stress Intensity Factors as a Function of Position Along Flaw Front.....13

ABSTRACT

In support of probabilistic fracture mechanics (PFM) studies for the High Flux Isotope Reactor (HFIR) Vessel Life Extension Program, a stress analysis of the HB-2 beam tube has been carried out to calculate linear-elastic fracture mechanics (LEFM) stress intensity factors for postulated corner flaws. Employing the ORNOZL mesh generation code and the ABAQUS stress-analysis code, 3-dimensional finite-element models of the HB-2 nozzle with corner flaw radii ranging from 0.5 in. – 1.5 in. were built and analyzed.

1. INTRODUCTION

In support of probabilistic fracture mechanics (PFM) studies [1] for the High Flux Isotope Reactor (HFIR) Vessel Life Extension Program, an extension of a previous stress analysis [2] of the HB-2/HB-3 beam tubes has been carried out to calculate linear-elastic fracture mechanics (LEFM) stress intensity factors for postulated corner flaws in HB-2.

The HFIR, located at Oak Ridge National Laboratory (ORNL), is a beryllium-reflected, light-water-cooled and –moderated, flux-trap type reactor that uses highly enriched ^{235}U as the fuel [3]. Figure 1 shows a vertical cross-section of the HFIR pressure vessel including the fuel core, beryllium reflector, engineering facilities, and beam tubes. The HFIR is equipped with three horizontal beam tubes, extending outward from the reactor core midplane as shown in the horizontal cross-section of the pressure vessel in Fig. 2. The HB-2 beam tube extends radially from the reactor center line with its inner end penetrating the permanent reflector. Also penetrating the permanent reflector, the HB-3 beam tube extends tangentially from the core, and the remaining beam tube is positioned on a tangential line with its ends designated as HB-1 and HB-4.

Proposed upgrades of the HFIR experimental facilities include increasing the diameters of the HB-2 and HB-4 beam tubes. These changes tend to result in higher radiation exposure rates in the vicinity of the beam-tube nozzles by reducing the amount of water between the beam tube and the nozzle [1]. For the upgrade design, the relatively high dose rate at the HB-2 nozzle corner makes this location dominant (relative to HB-4) in PFM studies, thus motivating a detailed calculation of HB-2 nozzle corner stress intensity factors (applied K_I). The results of 3-dimensional LEFM finite-element analyses of postulated HB-2 corner flaws are reported herein.

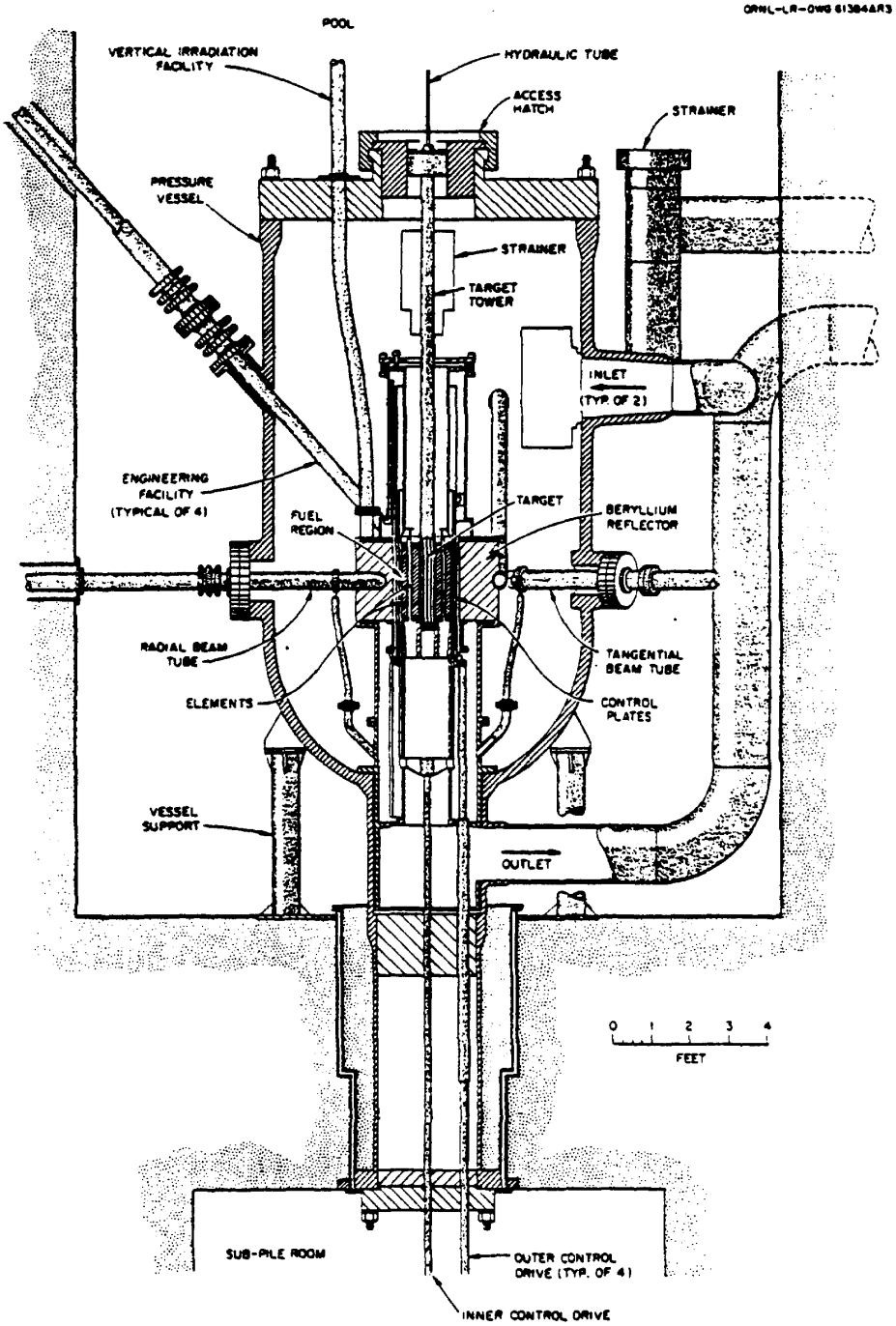

Fig. 1. Vertical cross-section of HFIR pressure vessel including core, beryllium reflector, engineering facility, and beam tubes.

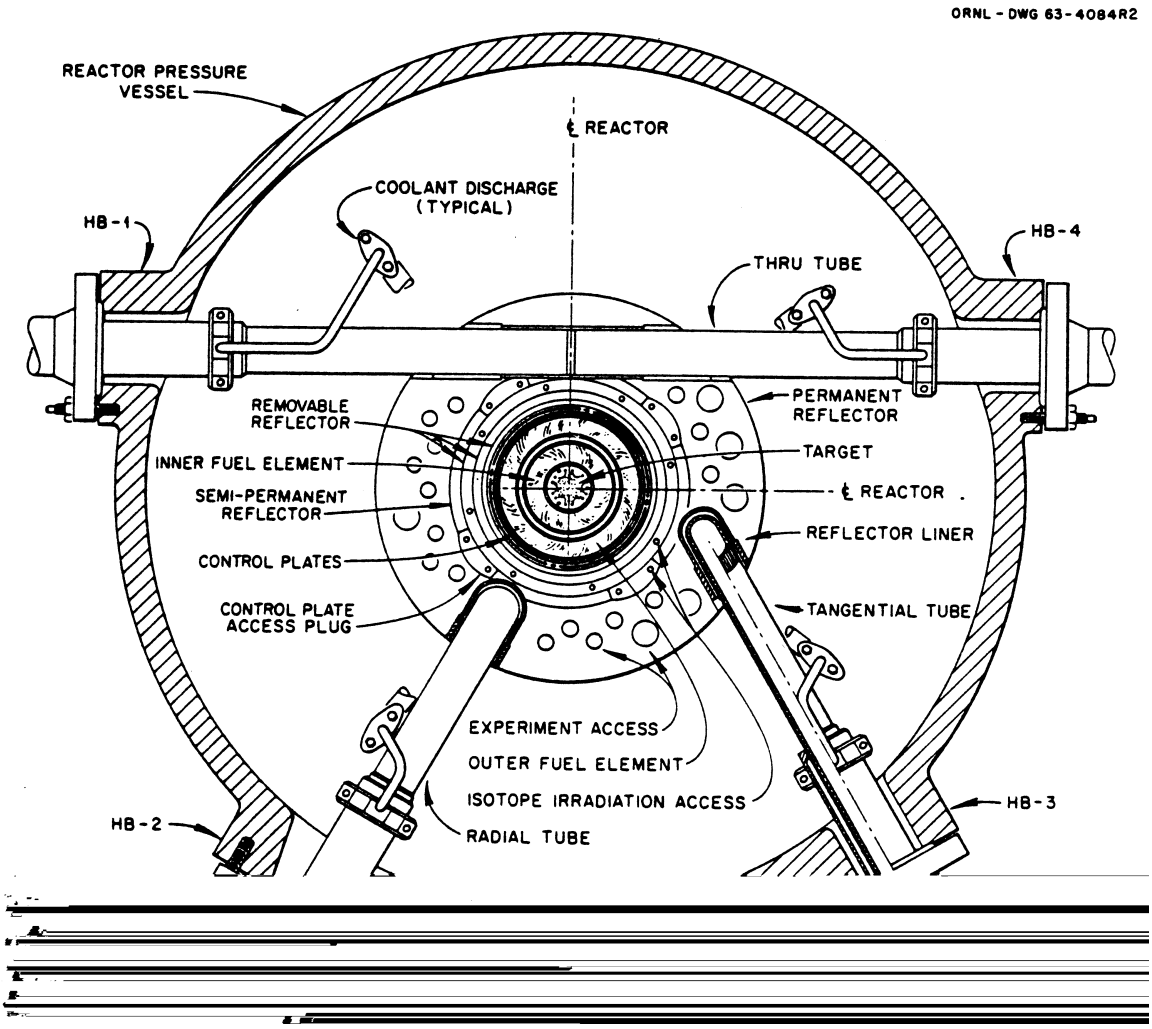

Fig. 2. Horizontal cross-section of HFIR pressure vessel and core at horizontal midplane of core.

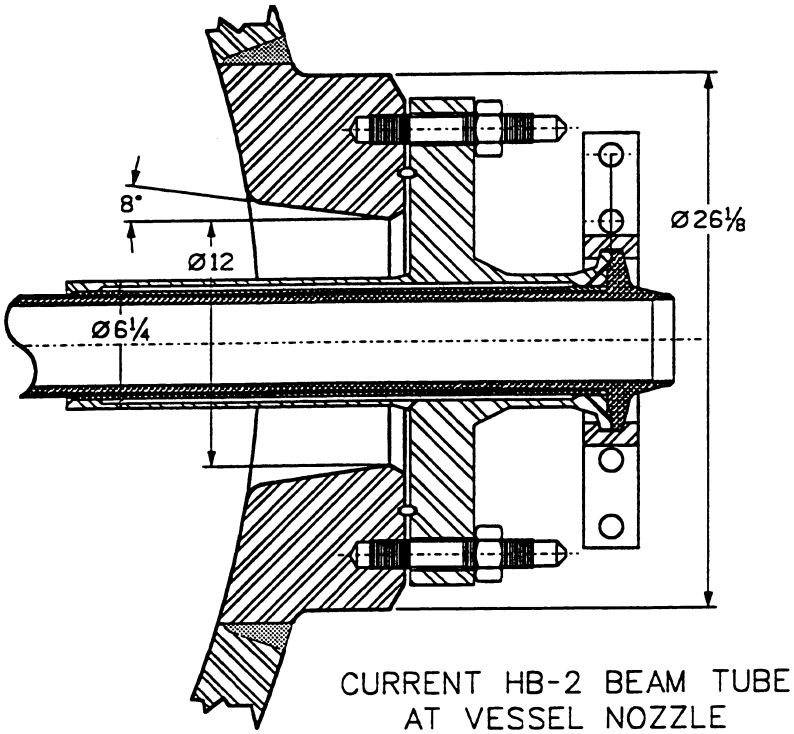

(a)

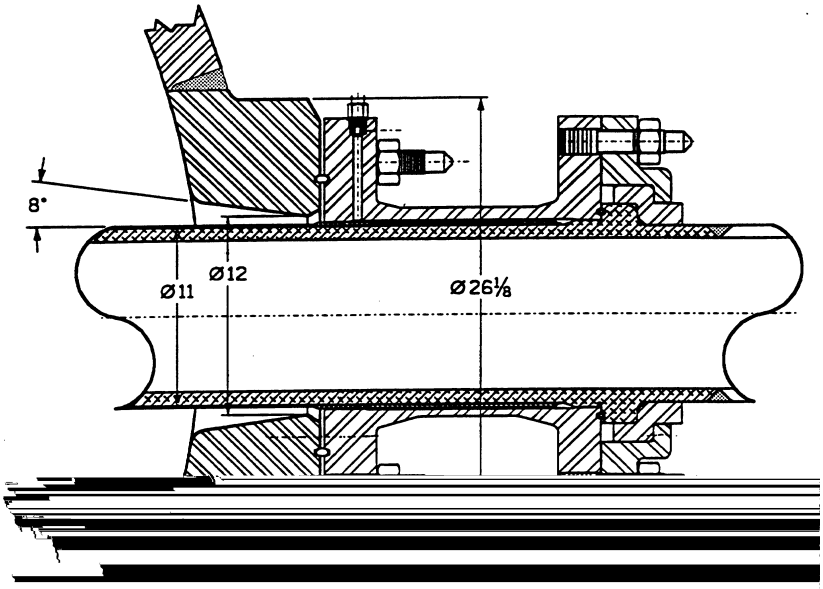

(b)

Fig. 3. (a) Present and (b) new designs of HB-2 beam tube at nozzle location (from [1]).

2. FINITE-ELEMENT MODELS

2.1 GEOMETRY

Figure 4 shows a layout of the simplified geometry of a postulated corner flaw used to construct the finite-element models. These simplifications were necessary to allow the effective use of the ORNOZL [4] finite-element mesh generator code. ORNOZL was designed to automatically create 3-dimensional finite-element meshes for four configurations of a corner crack in a nozzle-vessel intersection. The code generates a core of special wedge or collapsed prism elements at the crack front to introduce the appropriate stress singularity at the crack tip for LEFM analyses. Regular 20-node triquadratic isoparametric hexahedral elements are used away from the crack front. An option is also included to produce an embedded or penetrating flaw in clad materials.

In Fig. 4, the geometric variables input to ORNOZL for the HB-2 nozzle were:

r_v = vessel radius = 47.125 in.
r_i = nozzle radius = 7.0 in.*
t_{clad} = inner cladding thickness = 0.125 in.
t_{wall} = wall thickness = 3.125 in.**

*a constant nozzle radius is required by ORNOZL
**wall thickness includes 0.125 in. of cladding

A range of corner flaw geometries were investigated with their dimensions given in Table 1.

Table 1. Corner Flaw Geometries

Flaw Radius, r_F (in.)	Flaw Depth, a (in.)	Corner Radius, r_c (in.)
0.25	0.209	0.10
0.50	0.397	0.25
0.75	0.647	0.25
1.00	0.793	0.50
1.25	1.043	0.50
1.50	1.230	0.50

The variation in corner flaw radius, r_c, was required to stay within the geometry constraints of the ORNOZL code and does not reflect variations in the HB-2 design. Figure 5 shows a general mesh layout produced by ORNOZL for a 90-degree ¼-model. The lower horizontal and the two vertical planes are treated as reflective symmetry planes (excluding the crack face), thus implying a four-fold symmetry. Since the implied additional flaws are too far apart to interact, their presence does not affect the results of the analysis. The nodes in the upper horizontal plane in Fig. 5 are constrained to displace in-plane through the application of multi-point constraints (MPC). A closeup of the six corner flaws investigated in the analysis are shown in Fig. 6.

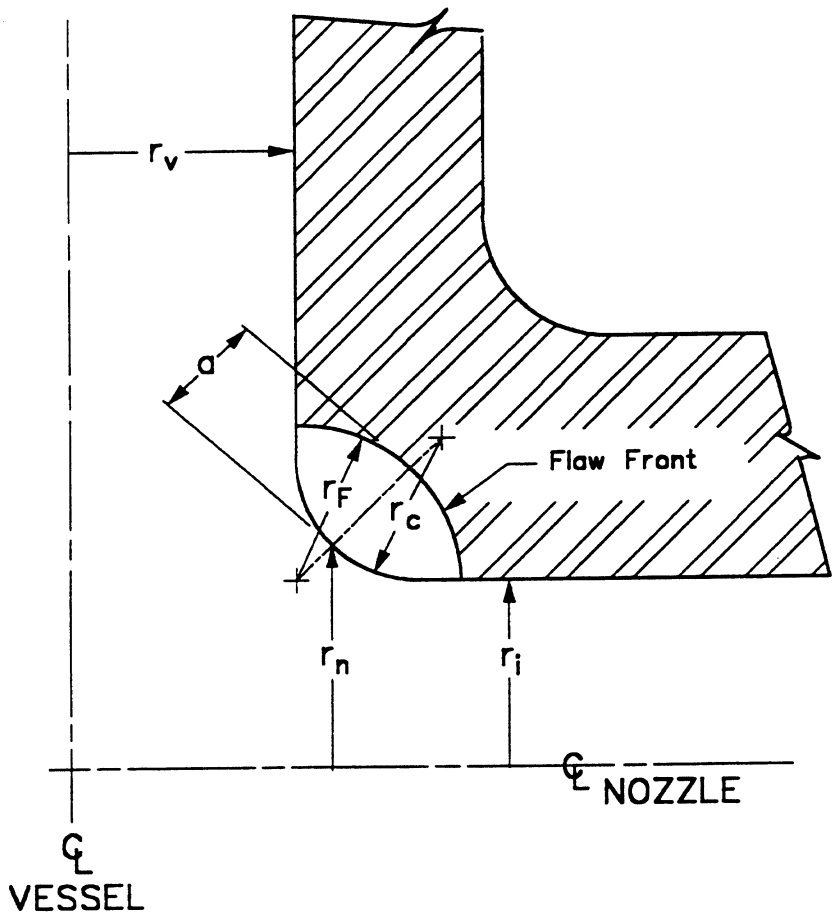

Fig. 4. Nozzle corner flaw with geometric variables defined (from [1]).

Fig. 5. General mesh layout for 90 degree model of HB-2 corner flaw: 2442 quadratic 20-node elements and 11,700 nodes.

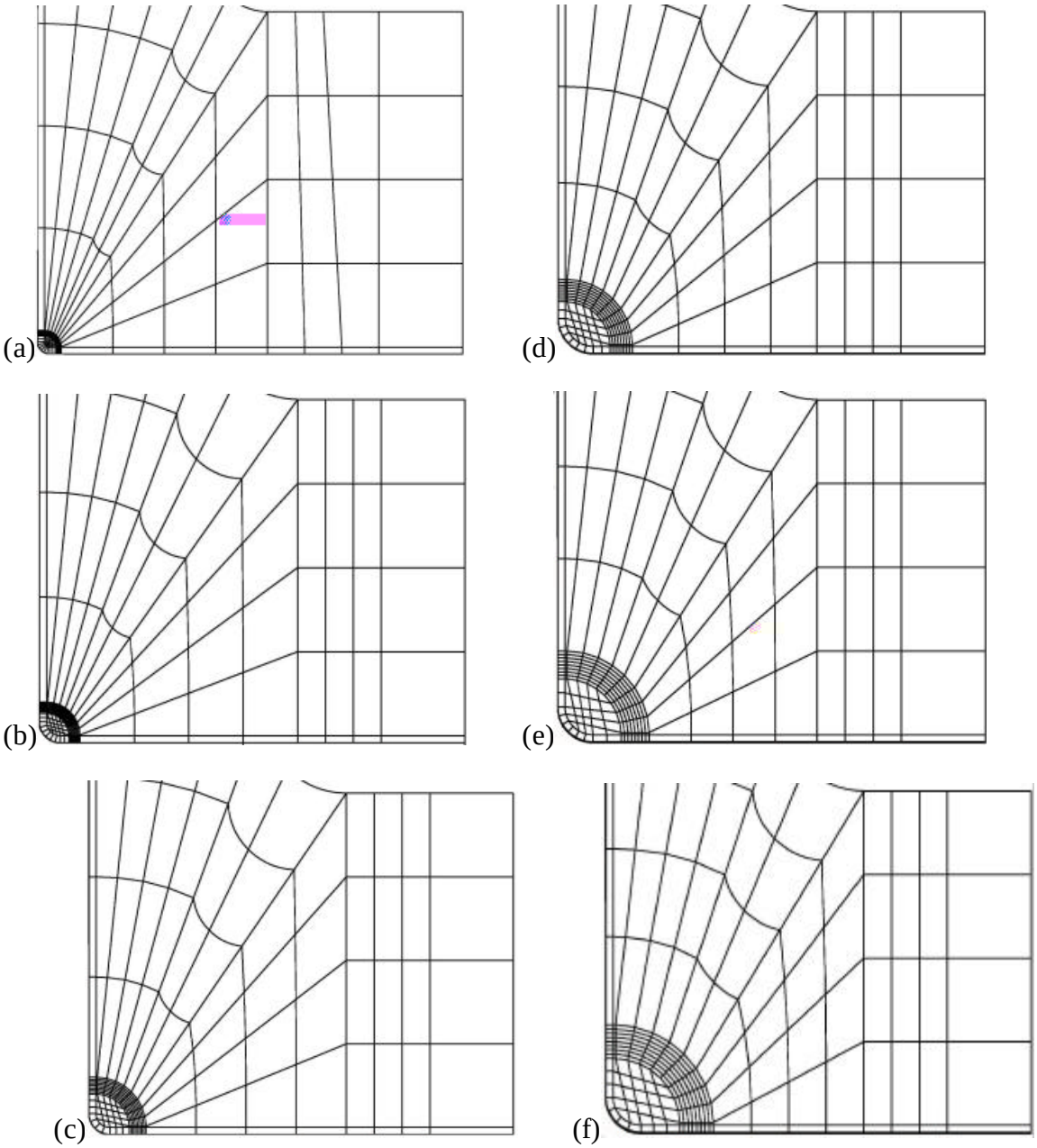

Fig. 6. Mesh layouts of six corner flaws: (a) r_F = 0.25 in. (b) r_F = 0.5 in. (c) r_F = 0.75 in. (d) r_F = 1.0 in. (e) r_F = 1.25 in. (f) r_F = 1.5 in.

2.2 MATERIAL PROPERTIES

The constant linear-elastic material properties used in the analyses are given in Table 2.

Table 2. Material Properties

Property	Base	Cladding
Young's Modulus, *E* (ksi)	28 000	22 800
Poisson's Ratio, ν	0.3	0.3
Coeff. of Thermal Expansion, α (°F^{-1})	7.77×10^{-6}	9.45×10^{-6}

2.3 THERMAL AND MECHANICAL LOADING

For all flaw geometries, the mechanical loading included an internal pressure of 0.9 ksi applied to all inner surfaces of the vessel and nozzle. In addition a longitudinal axial traction tensile load of 6.993 ksi was applied to the upper horizontal surface (see Fig. 5) to simulate the "blow-off" load resulting from the reactor pressure vessel being capped off at both ends. A thermal-differential-expansion stress in the cladding of 25 ksi was established by setting the stress-free temperature at 500 °F and then lowering the temperature of the vessel to 30 °F. These thermal and mechanical loadings produced the opening-mode stress profiles along the flaw front shown in Fig. 7.

2.4 ABAQUS QUALITY ASSURANCE

All stress analysis and *J*-integral calculations were carried out using the ABAQUS/ Standard, (version 5.7-1) [5] code on an IBM Risc/6000 Model 560 workstation computer running under the AIX operating system 4.2.1.0. The developers of ABAQUS, (Hibbit, Karlson, and Sorenson, Inc., (HKS)) have implemented a Quality Assurance Plan that is based on the ANSI/ASME NQA-1 Quality Assurance standard, which is designed to ensure compliance with Appendix B of US federal regulation 10 CFR 50 (1-1-86). HKS contracts annually with an independent quality assurance audit organization to audit HKS's quality assurance procedures. The audit organization is chosen for its experience and its ability to ensure that HKS complies with the provisions of the ISO 9001:1994 and NQA-1 quality standards. ABAQUS is certified under ISO 9001 Certificate No. A3897 issued by the Underwriters Laboratory, Inc. ® (issue date: April 9, 1996; revision date: March 9, 1998; renewal date: April 9, 2000).

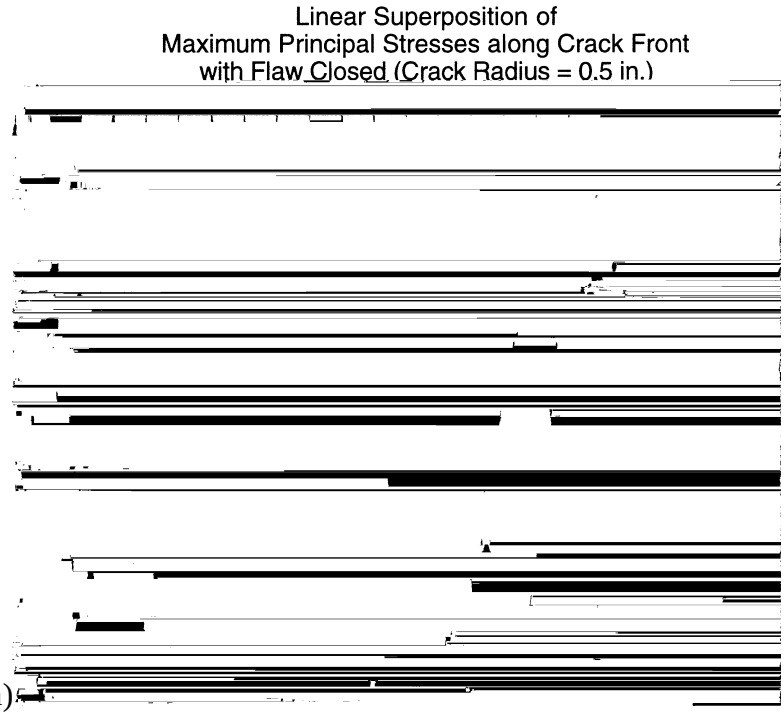

(a)

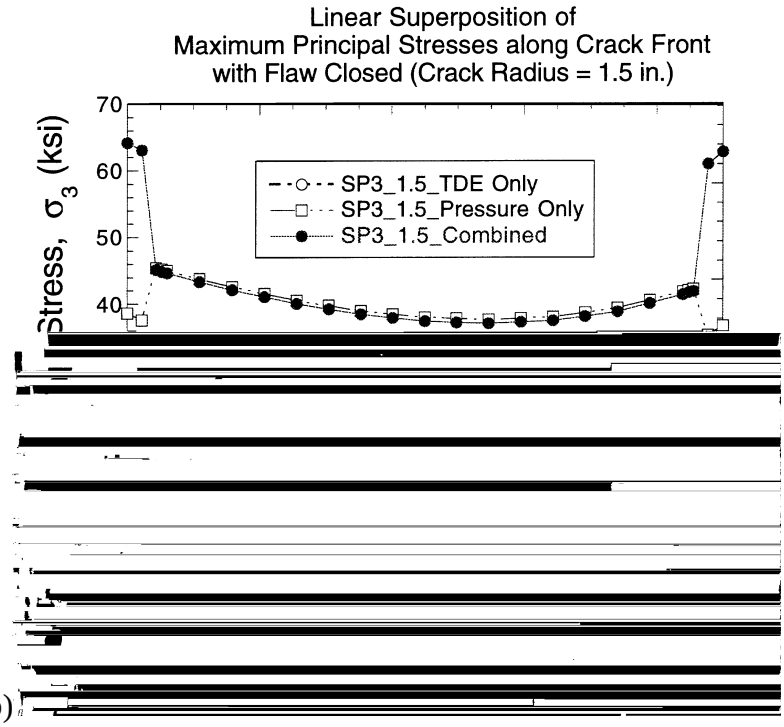

(b)

Fig. 7. Contributions to maximum principal (opening-mode) stresses along nozzle-corner flaw front for flaw radii of (a) 0.5 in. and (b) 1.5 in.

2.5 STRESS INTENSITY FACTORS

The current methodology for applying finite-element modeling of both linear elastic fracture mechanics (LEFM) and elastic-plastic fracture mechanics (EPFM) problems typically involves the calculation of the *J*-integral as a characterization of the *crack driving force*. Finite-element stress analysis codes such as ABAQUS [5] calculate this fracture mechanics parameter by the Domain Integral Method [6,7]. For linear elastic analyses, LEFM Mode I stress intensity factors, K_I, can readily be determined from the energy release rate interpretation of the *J*-integral given specific assumptions regarding the stress state near the crack tip.

Irwin [8] showed in 1957 that the Mode I stress intensity factor K_I is related to the elastic strain energy release rate, *G*, by

$$K_I^{\ 2} = E^* G \tag{1}$$

where the elastic modulus, *E**, for *plane stress* is

$$E^* = E \tag{2}$$

and for *plane strain*

$$E^* = \frac{E}{\left(1 - n^2\right)} \tag{3}$$

In Eqs. (2) and (3), *E* is Young's modulus and ν is Poisson's ratio. Under the conditions of LEFM, it has been shown [9] that the *J*-integral is equivalent to the elastic strain energy release rate, i.e., *J* = *G*, and from Eq. (1), therefore,

$$K_I = +\sqrt{E^* J} \tag{4}$$

It is a common convention to use Eqs. (3) and (4) (i.e., plane strain conditions) to convert *J*-integral results into linear-elastic Mode I stress intensity factors, i.e.,

$$K_I = +\sqrt{\frac{E\,J}{\left(1 - n^2\right)}} \tag{5}$$

Eq. (5) was applied for all of the stress intensity factors reported herein. Recognizing that, for 3-dimensional stress fields, the plane strain assumption is an approximation, the application of the plane strain conversion represents a conservative upper bound for the resulting stress intensity factors.

3. RESULTS AND DISCUSSION

Stress intensity factors were calculated for the flaw geometries, material properties, and loading conditions described in Sects. 2.1-3. The results are plotted in Fig. 8 as a function of crack tip angle. The effects of the cladding (with its associated residual stress and material properties) were investigated for two flaw radii, 0.5 in. in Fig. 9 and 1.5 in. in Fig. 10. As can be observed in Fig. 8, increasing flaw radii produces higher stress intensity factors where the peak K_J occurs either at the inner surface or for larger flaws near the clad/base interface. Peak stress intensity factors are presented in Table 3. The presence of the cladding (Figs. 9 and 10) elevates the stress intensity factor along the complete flaw front. Table 4 presents the results of all of the flaw radius cases with the cladding included.

Table 3. Peak Stress Intensity Factors

Flaw Radius (in.)	Flaw Depth (in.)	K_J ksi-√in.
0.25	0.209	44.1
0.50	0.397	59.1
0.75	0.647	70.3
1.00	0.793	76.5
1.25	1.043	82.9
1.50	1.293	88.3

4. SUMMARY

Stress intensity factors have been calculated for the HB-2 nozzle corner. Employing the ORNOZL mesh generation code and the ABAQUS stress-analysis code, 3-dimensional finite-element models with corner flaw radii ranging from 0.5 in.-1.5 in. were built and analyzed for a single loading condition. This study was carried out as a part of the High Flux Isotope Reactor (HFIR) Vessel Life Extension Program.

ACKNOWLEDGMENTS

During the course of this study, R. D. Cheverton provided valuable consultation and advice. His contributions are gratefully acknowledged by the authors.

Table 4. Stress Intensity Factors as a Function of Position Along Flaw Front

Flaw Radius = 0.25 in.				Flaw Radius = 0.75 in.				Flaw Radius = 1.25 in.			
ncrk	angle	K_J	J	ncrk	angle	K_J	J	ncrk	angle	K_J	J
1	0.00	48.94	0.095610	1	0.00	70.69	0.199452	1	0.00	80.11	0.256163
3	18.43	39.71	0.062943	3	8.13	63.15	0.159184	3	5.19	74.82	0.223450
5	19.51	41.18	0.055100	5	9.64	65.76	0.140552	5	6.81	77.53	0.195338
7	25.94	35.45	0.040833	7	18.61	56.45	0.103557	7	16.47	66.12	0.142087
9	32.33	33.57	0.036617	9	27.47	52.97	0.091204	9	26.03	61.66	0.123579
11	38.67	32.70	0.034749	11	36.26	51.40	0.085857	11	35.53	59.42	0.114730
13	45.00	32.45	0.034217	13	45.00	50.88	0.084147	13	45.00	58.46	0.111080
15	51.33	32.56	0.034454	15	53.74	51.11	0.084884	15	54.47	58.58	0.111514
17	57.67	33.27	0.035965	17	62.53	52.42	0.089311	17	63.97	60.08	0.117309
19	64.06	34.94	0.039671	19	71.39	55.68	0.100763	19	73.53	63.94	0.132858
21	70.49	40.26	0.052681	21	80.36	64.80	0.136484	21	83.19	74.87	0.182179
23	71.57	38.78	0.060031	23	81.87	62.29	0.154864	23	84.81	72.47	0.209606
25	90.00	47.73	0.090931	25	90.00	70.12	0.196219	25	90.00	78.41	0.245363

Flaw Radius = 0.50 in.				Flaw Radius = 1.00 in.				Flaw Radius = 1.50 in.			
ncrk	angle	K_J	J	ncrk	angle	K_J	J	ncrk	angle	K_J	J
1	0.00	61.77	0.152300	1	0.00	75.27	0.226098	1	0.00	84.21	0.283014
3	11.31	53.17	0.112837	3	6.34	68.89	0.189406	3	4.40	79.82	0.254305
5	12.69	55.33	0.099511	5	7.91	71.53	0.166269	5	6.05	82.56	0.221528
7	20.90	47.55	0.073475	7	17.31	61.18	0.121641	7	15.89	70.24	0.160358
9	29.00	44.84	0.065357	9	26.60	57.23	0.106434	9	25.64	65.23	0.138282
11	37.01	43.74	0.062166	11	35.82	55.41	0.099768	11	35.33	62.54	0.127118
13	45.00	43.21	0.060689	13	45.00	54.73	0.097351	13	45.00	61.22	0.121786
15	52.99	43.54	0.061596	15	54.18	54.93	0.098057	15	54.67	61.21	0.121751
17	61.00	44.44	0.064195	17	63.40	56.34	0.103146	17	64.36	62.68	0.127698
19	69.10	46.96	0.071660	19	72.69	59.97	0.116862	19	74.11	66.69	0.144537
21	77.31	54.51	0.096575	21	82.09	70.07	0.159574	21	83.95	78.18	0.198624
23	78.69	52.38	0.109495	23	83.66	67.59	0.182353	23	85.60	75.90	0.229929
25	90.00	61.08	0.148925	25	90.00	74.39	0.220840	25	90.00	81.11	0.262598

J [in.-kips/in^2]
K_J [ksi-√in.]
angle [degrees]

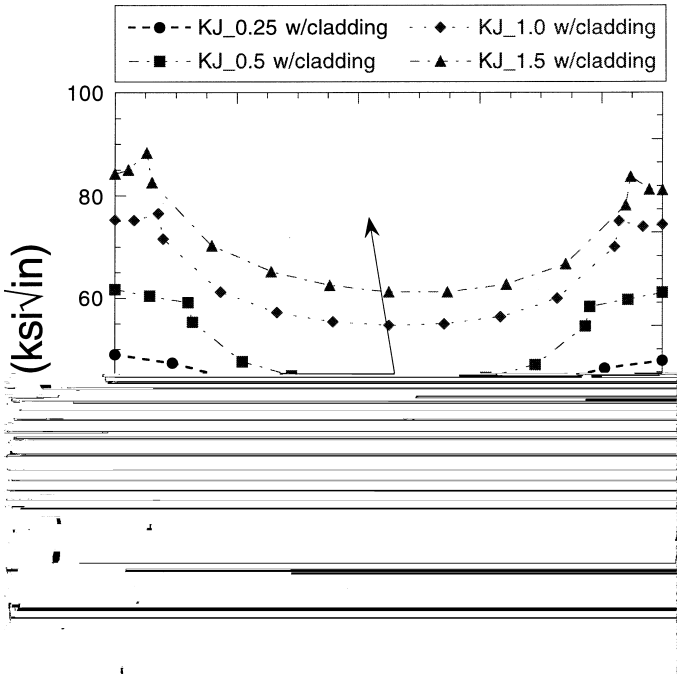

Fig. 8. Distribution of stress-intensity factors along flaw front for a range of flaw radii.

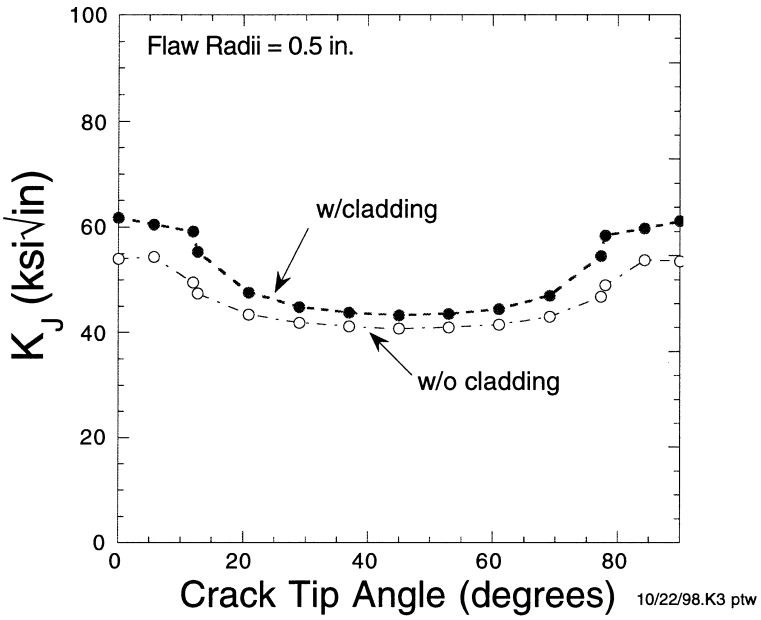

Fig. 9. Stress intensity factors along flaw front with and without cladding for a flaw radius of 0.5 in.

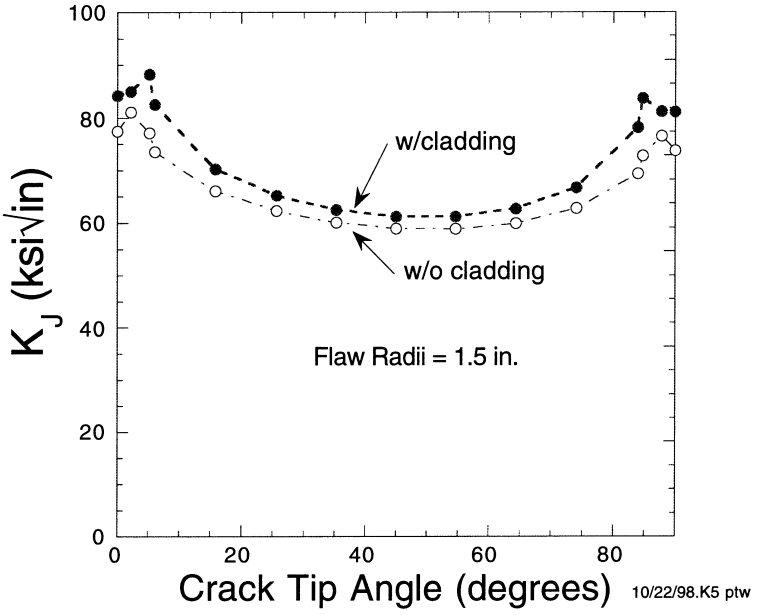

Fig. 10. Stress intensity factors along flaw front with and without cladding for a flaw radius of 1.5 in.

5. REFERENCES

[1] R. D. Cheverton and T. L. Dickson, *HFIR Vessel Life Extension with Enlarged HB-2 and HB-4 Beam Tubes*, ORNL/TM-13698, Lockheed Martin Energy Research, Oak Ridge Natl. Lab., December 1998.

[2] P. T. Williams, *Stress Analysis of the HFIR HB-2 and HB-3 Beam Tube Nozzles*, ORNL/TM-1998/9, Lockheed Martin Energy Research, Oak Ridge Natl. Lab., August 1998.

[3] *Operating Manual for the High Flux Isotope Reactor*, ORNL/TM-138/R1, Union Carbide Corp., Nuclear Division, Oak Ridge Natl. Lab., 1982.

[4] J. Keeney-Walker and B. R. Bass, *ORNOZL: A Finite-Element Mesh Generator for Nozzle-Cylinder Intersections Containing Inner-Corner Cracks*, NUREG/CR-5872 (ORNL/TM-11049), Martin Marietta Energy Systems, Inc., Oak Ridge Natl. Lab., September 1992.

[5] *ABAQUS Theory Manual, Version 5.7*, Hibbit, Karlson, and Sorenson, Inc., Providence, RI, 1997.

[6] F. Z. Li, C. F. Shih, and A. Needleman, "A Comparison of Methods for Calculating Energy Release Rates," *Engineering Fracture Mechanics*, **21**, (1985) 405-421.

[7] B. Moran and C. F. Shih, "A General Treatment of Crack Tip Contour Integrals," *International Journal of Fracture* **35**, (1987) 295-310.

[8] G. R. Irwin, "Analysis of Stresses and Strains Near the End of a Crack Traversing a Plate," *Journal of Applied Mechanics* **24**, (1957) 361-364.

[9] J. Rice, "A Path Independent Integral and the Approximate Analysis of Strain Concentration by Notches and Cracks," *Journal of Applied Mechanics* **16**, (1968) 1-12.

INTERNAL DISTRIBUTION

1-3. B. R. Bass
4. S. E. Burnette
5-6. R. D. Cheverton
7. S. J. Chang
8. K. W. Childs
9. D. H. Cook
10. T. L. Dickson
11. D. M. Hetrick
12-14. J. R. Inger
15. S. K. Iskander
16. M. A. Kuliasha
17. W. J. McAfee
18. L. D. Proctor
19. D. L. Selby
20-24. P. T. Williams
25. Research Reactors Division – DCC – RC
26. ORNL Patent Office
27-28. Central Research Library
29-30. Laboratory Records (for OSTI)
31. Laboratory Records, RC